Semiconductors, 2023, Vol. 57, No. 3

Oxide desorption process from InSb surface under Sb flux

© M.A. Sukhanov, A.K. Bakarov, K.S. Zhuravlev

Rzhanov Institute of Semiconductor Physics, Siberian Branch, Russian Academy of Sciences,
630090 Novosibirsk, Russia

E-mail: msukhanov@isp.nsc.ru

Received February 10, 2023
Revised March 30, 2023
Accepted April 10, 2023

In this work, the process of oxide removal from the InSb (001) surface was studied *in situ* by high-energy electron diffraction in vacuum and under an antimony flux. The dependence of the oxide thickness on the annealing temperature was obtained. It has been found that the antimony flux slows down the process of oxide removal due to the oxide formation reaction. The oxide removal process was described by a system of kinetic equations, the activation energy of oxide decomposition was determined

Keywords: InSb, oxide, activation energy, desorption.

DOI: 10.21883/SC.2023.03.56228.4580

1. Introduction

One of the most promising science-intensive technologies of the XXI century is thermal imaging. The basis of thermal imaging devices are matrix photodetectors of the IR range, which form an image. Semiconductor heterostructures based on InSb [1–3], which are usually grown on InSb substrates, are widely used to create matrix photodetectors in the mid-IR range ($3-5\,\mu$m). Before epitaxial growth, the substrates are cleaned and the oxide layer is removed from the surface, otherwise its residues lead to the formation of defects at the interface between the layer and the substrate [4]. Several methods are used to remove oxides from the InSb surface: surface treatment in various solutions [5,6], thermal annealing, surface exposure in a flow of molecular or atomic hydrogen [7], oxide removal by ion bombardment [8]. Exposure in a flow of hydrogen and antimony allows to obtain a smooth substrate surface morphology ($R_{ms} = 0.15$ nm) [9], but requires additional equipment. The most commonly used method for oxide removal is — thermal annealing in a growth chamber. The choice of conditions for the thermal removal of the oxide is complicated by the fact that the desorption of antimony and indium oxides from the surface occurs at temperatures close to the temperature of incongruent evaporation of InSb, so there is a opportunity of degradation of the substrate surface [10]. Thermal annealing without an antimony flow results in deterioration of the surface morphology, formation of InSb islands, surface faceting, degradation of the substrate, and formation of indium islands [11].

The process of oxide desorption in vacuum can be controlled by high-energy electron diffraction (HEED). In the paper [11] several stages of oxide removal were distinguished. At the beginning of annealing, there is a background with diffraction rings in the HEED pattern, then, as heating proceeds, desorption of antimony oxides occurs, reflections appear, possibly corresponding to diffraction in the In layer In_2O_3. In paper [12] two intervals of desorption were also distinguished. The first interval — desorption of antimony oxides with the formation of additional diffraction reflections associated with indium oxides, and the second interval at higher temperatures — desorption of indium oxides. At the second interval, the intensity of indium oxide reflections decreases, and a reconstruction (1×3) is formed on the InSb surface. Only in the paper [12] the activation energy of 3.7 eV of the oxide removal process in vacuum at a constant substrate temperature was obtained, calculated from the time required to obtain a diffraction pattern without additional reflections associated with oxides. The obtained activation energy, apparently, is equal to the sum of the activation energies of the processes of removal of antimony oxides and indium oxides. The effect of the antimony flow on the oxide removal process has not yet been studied.

The purpose of this paper — *in situ* is to study the process of thermal desorption of oxides from the surface of InSb in vacuum and in an antimony flow, to determine the effect of the antimony flow on the rate and activation energy of the oxide decomposition process.

2. Experiment procedure

The oxide was removed from the epi-ready InSb (001) substrates by thermal annealing in the growth chamber of a molecular beam epitaxy (MBE) Compact-21T (Riber) unit. Before loading into the growth chamber, the substrate was annealed in a buffer vacuum chamber at a temperature of $T = 175^\circ$C for 30 min. In the growth chamber, the substrate was heated from room temperature to $T = 370^\circ$ at a rate of 10°C/min, then to $T = 400^\circ$C at a rate of 5°C/min. At a temperature of $T = 400^\circ$C, the sample was kept for 10 min to stabilize the temperature. Further heating of the sample was carried out at a rate of 5°C/min up to 450°C. Then the sample was kept at a constant temperature 450°C. The substrate temperature was controlled using a thermocouple.

The thermocouple temperature was preliminarily calibrated against the known temperature of the $(1 \times 3) \to c(4 \times 4)$ reconstruction transition on the InSb [13] surface. A valve source with a cracking zone was used as a source of antimony. At the chosen temperature of the cracking zone (800°C), the antimony flow consisted of a mixture of Sb atoms and dimers Sb_2 [14]. The antimony flux from the source was preliminarily measured using an ionization vacuum gauge placed directly in front of the substrate and was $3.3 \cdot 10^{-6}$ Torr, which is equivalent to the flow $2 \cdot 10^{14}$ at $\cdot$ cm$^{-2} \cdot$ c^{-1} [15]. The flow of antimony was supplied to the surface at a temperature of ~ 422.5°C. The process of oxide desorption was controlled *in situ* by high-energy electron diffraction. The angle of incidence of the electron beam was 3°, energy 12 keV. The HEED pattern was recorded and processed using the KSA400 system, which included a CCD camera and a processing program. The frequency of recording HEED patterns is 25 frames per second.

3. Experimental results

Initially, there was a diffuse background predominantly in the HEED pattern (Fig. 1, *a*), which indicates the presence of a rather thick layer of amorphous oxide on the InSb surface. As the temperature increased, the background intensity gradually decreased and the intensity of the fundamental HEED reflections of InSb increased (Fig. 1, *b*). From the very beginning of the registration of the fast electron diffraction pattern, already at $T = 410$°C the intensity of the fundamental 00 reflection exceeded

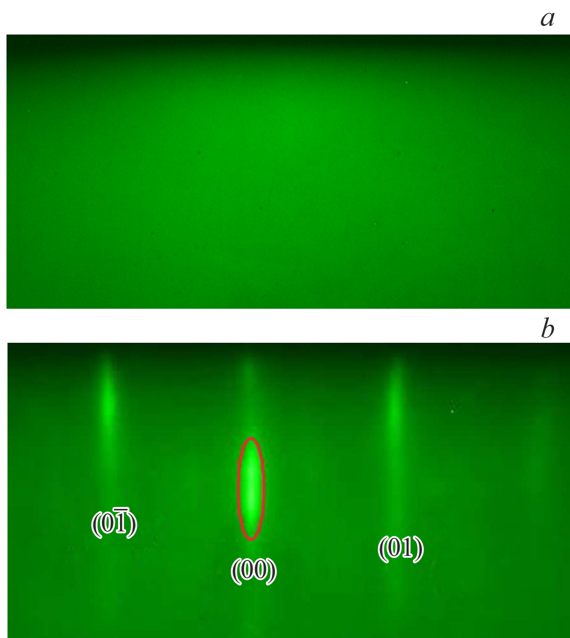

Figure 1. Fast electron diffraction pattern from the InSb surface: *a* — coated with oxide, *b* — after annealing at $T = 450$°C. The intensity of the red area was monitored.

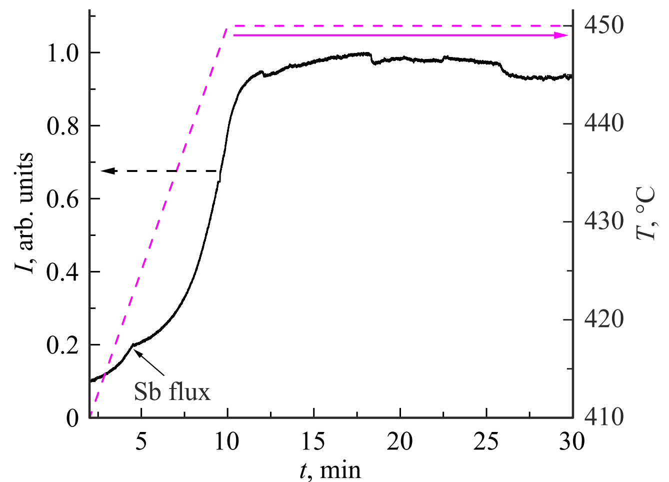

Figure 2. Dependence of the normalized intensity of the 00 diffraction InSb reflection on the annealing temperature and time. The InSb temperature is plotted on the right *y*-axis. The pink dotted line corresponds to the time-temperature dependence. (A color version of the figure is provided in the online version of the paper).

the background intensity. This allowed to determine the location of the 00 InSb reflection and areas free from InSb reflections. Since the purpose of the paper was to study the effect of the antimony flow, HEED patterns were first recorded without an antimony flow when the sample was heated in the range from $T = 410$ to $T = 422.5$°C, with subsequent heating of $T > 422.5$°C, HEED patterns were recorded in an antimony flow. Then, from the recorded films in the selected region of the HEED pattern, the intensity kinetics of the 00 InSb reflection was obtained.

Figure 2 shows the increase in the intensity of the reflection 00 from the surface of InSb during heating. When a flow of antimony was applied, the intensity of the main reflection continued to grow, but the growth rate decreased. After reaching $T = 450$°C, the sample was kept for 20 min at a constant temperature in an antimony flow to completely remove the oxide. After the final temperature was reached, the intensity of the main reflection continued to grow for 2 min to a certain constant value. Similarly, the intensity of other main reflections increased. The background intensity, which was measured far from reflections, decreased with time.

At the beginning of the experiment, the diffraction pattern is a smooth background, which indicates that the oxide layer is thick enough to scatter the electron beam and, accordingly, reduce its intensity. When passing through a layer with a thickness of S, the intensity of the electron beam decreases due to scattering according to the law:

$$I = I_0 e^{-S/\lambda}, \quad (1)$$

where λ — the mean free path of electrons before scattering, which generally depends on the energy of electrons and the material [16,17]. In the HEED geometry, the electron

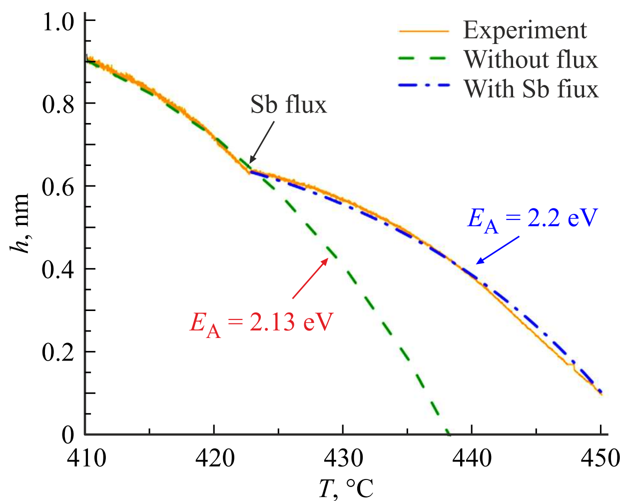

Figure 3. Dependence of oxide thickness on temperature. Experiment (orange solid line), calculation by formula (3) in vacuum (green dashed line) and in an antimony flow (blue dash-dotted line).

beam is incident on the sample surface at an angle 3°, the electrons pass through the oxide twice, before and after diffraction on the crystal, therefore

$$S = \frac{2h}{\sin(\theta)}. \qquad (2)$$

Here θ — beam incidence angle, h — oxide thickness. Accordingly, from the change in the intensity of the reflection, knowing the length of the electron path, the thickness of the oxide through which the electron beam passes can be estimated. There are no data on the electron path lengths in the oxides Sb_2O_3, Sb_2O_5 and In_2O_3 in the literature. The mean free path in indium and antimony oxides can be estimated using the formula (modified Bethe equation) [18,19]. The path length generally depends on the density of the material, the electron energy, the molar mass, the number of valence electrons, and the band gap. For oxides of indium and antimony, the estimate of the mean free path of electrons gives the average value $\lambda \approx 15$ nm.

The intensity of the central reflection increases as the oxide is desorbed from the InSb surface and, accordingly, the scattering of electrons in the oxide layer decreases. Figure 3 shows the dependence of the oxide layer thickness on the annealing temperature (orange curve) obtained from the 00 reflection intensity kinetics (Fig. 2) using formulas (1) and (2). The resulting thickness of the oxide layer is the effective thickness, since as the oxide is removed, the coating ceases to be continuous and obtains a fragmentary character. In the model used, the scattering in the case of a fragmentary coating is equivalent to the scattering of an electron beam in an oxide of effective thickness. The resulting dependence was approximated by a formula describing the effective rate of the oxide removal reaction:

$$\frac{dh}{dt} = -k, \qquad (3)$$

where $k = Ae^{-\frac{E_A}{k_B T}}$ — effective oxide removal rate constant, described by the Arrhenius law, A — frequency factor, E_A — activation energy of the oxide removal process. The value of E_A before and after turning on the antimony flow is 2.13 (green dotted line) and 2.2 eV (blue dashed line), respectively, with a frequency factor of $A = 10^{13}\ c^{-1}$. An increase in activation energy means a decrease in the rate of oxide removal.

The decrease in the rate of oxide removal when the antimony flow is supplied may be due to the influence of the reverse reaction of oxide formation, or the fact that antimony interferes with the removal of oxide.

4. Results and discussion

Since antimony oxide decomposes in the first interval of oxide removal, and indium oxide removal requires the substrate to be kept at higher temperatures for a long time [12], we can initially consider only the antimony oxide decomposition process. Indium oxide after the removal of antimony oxide apparently remains in the form of nanocrystals rather than a continuous film [4], so the intensity of the diffraction reflection saturates. The process of thermal decomposition of antimony oxide into antimony and oxygen is described by the reactions [11]:

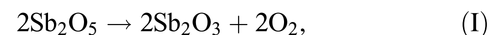

$$2Sb_2O_5 \rightarrow 2Sb_2O_3 + 2O_2, \qquad (I)$$

$$2Sb_2O_3 \rightarrow 4Sb + 3O_2. \qquad (II)$$

After the decomposition of antimony oxide, oxygen and antimony are released, which can again form antimony oxide due to the reverse reaction or desorb from the surface.

To describe the process of oxide decomposition and, accordingly, reduce its thickness, a system of differential equations (5)−(7) was numerically solved, describing the change in the amount of Sb_2O_3 (N_{ox}) (5), antimony (N_{Sb}) (6) and oxygen (N_{O_2}) (7) depending on the heating temperature and holding time at a constant temperature. The equations include chemical reactions of decomposition, formation of oxide Sb_2O_3, desorption of antimony atoms and oxygen molecules from the surface, the reaction rate constants $K(T)$ of which in the system of equations are denoted by indices diss, form, des. Sb and des. O, respectively, as well as the flow of antimony to the surface (F). The decomposition reaction for Sb_2O_3 was considered, since the intensity of the diffraction reflection increases during the reaction II, while during the reaction I, antimony oxide Sb_2O_5 passes into antimony oxide Sb_2O_3, which practically does not change the beam scattering in the oxide film in view of the previously given estimate for the mean free path of electrons in antimony oxides:

$$\frac{dN_{ox}}{dt} = -2K_{diss}(T)N_{ox}^{m}(t) + 2K_{form}(T)N_{Sb}(t)N_{O_2}(t), \qquad (5)$$

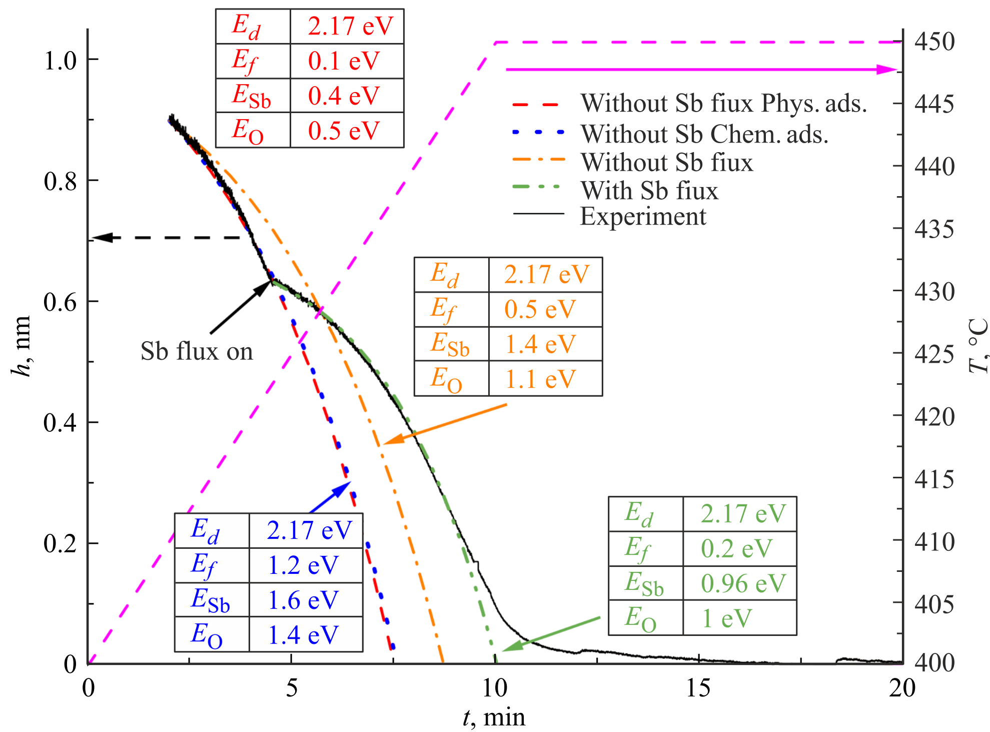

Figure 4. Experimental and design dependences of the oxide thickness on the temperature and annealing time for various reaction parameters. The InSb temperature is plotted on the right y-axis. The pink dotted line corresponds to the temperature dependence.

$$\frac{dN_{\text{Sb}}}{dt} = 4K_{\text{diss}}(T)N^m_{\text{ox}}(t) - 4K_{\text{form}}(T)N_{\text{Sb}}(t)N_{\text{O}_2}(t) - K_{\text{des.Sb}}(T)N_{\text{Sb}}(t) + F, \quad (6)$$

$$\frac{dN_{\text{O}_2}}{dt} = 3K_{\text{diss}}(T)N^m_{\text{ox}}(t) - 3K_{\text{form}}(T)N_{\text{Sb}}(t)N_{\text{O}_2}(t) - K_{\text{des.O}}(T)N_{\text{O}_2}(t). \quad (7)$$

In the system of equations, the decomposition reaction of antimony oxide was calculated for orders 0 and 1 ($m = 0, 1$), i.e., when the decomposition rate either does not depend on its own concentration or is proportional to the first power of the oxide's own concentration. The antimony flow (F) in the equations was taken equal to the value $3.3 \cdot 10^{-6}$ Torr, measured by an ionization vacuum gauge, which is equivalent to the flux density $2 \cdot 10^{14}\,\text{cm}^{-2} \cdot \text{c}^{-1}$. The value of 0.64 nm [20] was taken as an oxide monolayer. The reaction rate constants were calculated according to the Arrhenius law. The order of the desorption reaction of oxygen molecules and antimony atoms was assumed to be 1, the frequency factor in the reaction rate constants was taken equal to its characteristic value $10^{13}\,\text{c}^{-1}$ [21]. The activation energies of chemical reactions were determined by approximating the experimental dependences of the oxide thickness on the annealing temperature by solving the system of equations (5)–(7). Two cases were considered — physical or chemical adsorption of oxygen molecules and antimony atoms formed after the decomposition of the oxide or deposited from the flow on the surface of InSb or oxide.

First, the section of the curve without antimony flow ($F = 0$) was described. This area is described at zero order of the antimony oxide decomposition reaction. During physical adsorption, the desorption energies of antimony and oxygen from the surface are hundreds of meV [22]. The calculation shows that at desorption energies of 400 and 500 meV for antimony ($E_{\text{des.Sb}}$) and oxygen ($E_{\text{des.O}}$), respectively, the determining factor is the oxide decomposition energy (E_d). The design curve describes the experimental dependence at $E_d = 2.17$ eV (red dotted line in Fig. 4). The activation energy of oxide formation (E_{form}), even at low values, ≤ 200 meV, does not affect the rate of oxide removal, since the initial elements are easily desorbed. The oxide formation reaction does not affect the design dependence up to $E_{\text{des.Sb}}$ and $E_{\text{des.O}} \sim 1$ eV. With a further increase in $E_{\text{des.Sb}}$ and $E_{\text{des.O}}$ to the values corresponding to chemical adsorption, the reaction of oxide formation begins to decrease the rate of oxide removal (orange dash-dotted line in Fig. 4). To agree with the experiment, it is necessary to increase E_{form} or decrease E_d (dashed blue curve in Fig. 4), in this case a new set of energies appears that describe the experiment. Thus, when approximating the dependence without the antimony flow, it is impossible to determine the activation energies of reactions due to the mutual dependence between the activation energies of various chemical reactions. Both physically and chemically adsorbed oxygen and antimony atoms satisfy the experimental data.

When analyzing the area with an antimony flow ($F \neq 0$), the activation energies of the reaction were also varied within the limits corresponding to physical and chemical adsorption. The area with an antimony flow, similarly to the area without a flow, is described at zero order of the antimony oxide decomposition reaction. At $E_{\text{des.Sb}}$ and $E_{\text{des.O}}$ up to a value of ~ 1 eV, the antimony flow does not affect the rate of removal of antimony oxide even at low $E_{\text{form}} \sim 200$ meV. Accordingly, to reduce the oxide removal rate when an antimony flow is supplied, antimony and oxygen should be chemically adsorbed on the surface with $E_{\text{des.Sb}}$ and $E_{\text{des.O}} \geq 1$ eV. By varying E_d and E_{form}, the experimental dependence can be described in the antimony flow (green curve in Fig. 4). Analyzing only the area with an antimony flow, it is possible to exclude the values of $E_{\text{des.Sb}}$ and $E_{\text{des.O}} \leq 1$ eV, however, the uncertainty in the values of the activation energies of the processes of desorption of the products of the reaction of oxide decomposition and oxide formation remains.

It was shown in the paper [23] that the desorption energy of antimony at the frequency factor $10^{13}\,\text{c}^{-1}$ was $E_{\text{des.Sb}} = 1.6$ eV. This value corresponds to chemical adsorption and is included in the energy range established above; therefore, this value was used in further calculations. The analysis showed that the energies of decomposition E_d and formation of antimony oxide E_{form}, which determine the rates of the corresponding reactions, affect the rate of oxide removal without a flow and in an antimony flow to a different extent. The value of E_d affects the process rate in the same way in both cases, and E_{form} affects the process rate in the antimony flow more strongly due to an increase in the antimony concentration on the surface. As a result, for E_d there is a narrow range of possible values of $2.15 < E_d < 2.18$ eV, at which E_{form} and $E_{\text{des.O}}$ can be chosen, allowing to describe the experimental dependence. At $2.18 \leq E_d$ or $E_d \leq 2.15$there are no parameters $E_{\text{des.O}}$ and E_{form}, at which the calculation describes both the area without a flow and with an antimony flow at the same time. For instance, Fig. 5 shows the design curve for $E_d = 2.15$ eV, $E_{\text{des.Sb}} = 1.6$ eV, $E_{\text{des.O}} = 1.3$ eV, and $E_{\text{form}} = 1.07$ eV. It can be seen that the contribution of the oxide formation reaction for the area with an antimony flow is too high and the oxide removal rate is lower than in the experiment, while the oxide removal rate in the area without an antimony flow is higher than in the experiment. Accordingly, to match the calculation and experiment at such energies, it is necessary to simultaneously increase the contribution of the formation reaction in the area without a flow and decrease it in the area with a flow, which is impossible. When choosing a value E_d, which is included in the specified range, for example, $E_d = 2.172$ eV, at $E_{\text{form}} = 1.14$ eV, $E_{\text{des.Sb}} = 1.6$ eV and $E_{\text{des.O}} = 1.3$ eV, the calculated dependence of the thickness on time describes the experiment (Fig. 6). Thus, for a given value of $E_{\text{des.Sb}} = 1.6$ eV and the obtained value of $E_d \approx 2.17$ eV, the energies E_{form} and $E_{\text{des.O}}$ at which the experimental data are described are interdependent. To agree the calculation

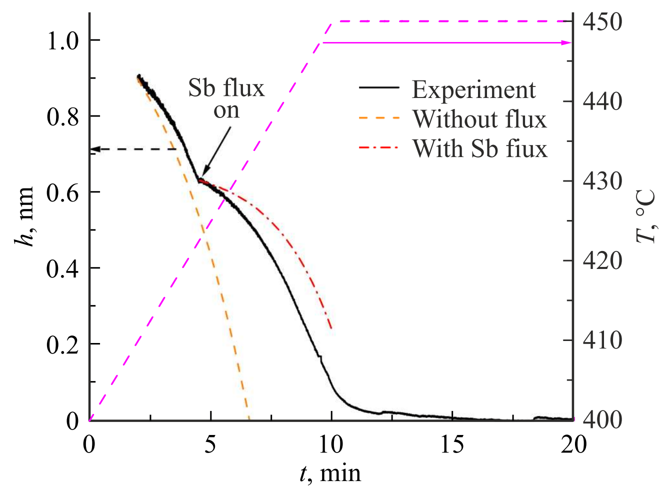

Figure 5. Experimental and design dependences of the oxide thickness on the temperature and annealing time at $E_{\text{des.Sb}} = 1.6$ eV, $E_{\text{des.O}} = 1.3$ eV, $E_d = 2.15$ eV and $E_{\text{form}} = 1.07$ eV. The temperature is plotted on the right y-axis. The pink dotted line corresponds to the time-temperature dependence.

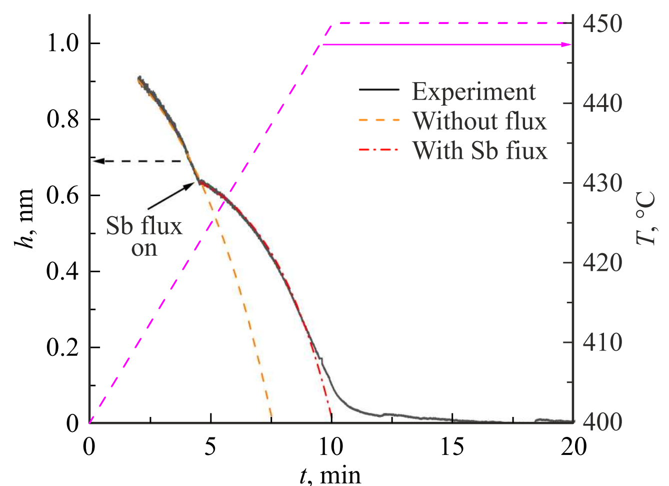

Figure 6. Experimental and design dependences of the oxide thickness on the temperature and annealing time at $E_{\text{des.Sb}} = 1.6$ eV, $E_{\text{des.O}} = 1.3$ eV, $E_d = 2.172$ eV and $E_{\text{form}} = 1.14$ eV. The temperature is plotted on the right y-axis. The pink dotted line corresponds to the time-temperature dependence.

and experiment, as $E_{\text{des.O}}$ increases, it is necessary to decrease the formation reaction rate (increase E_{form}), since the oxygen concentration increases. At $E_{\text{des.O}} \geq 2$ eV it is impossible to choose E_{form} for which the calculation describes the experiment. If E_{form} and $E_{\text{des.O}} \gg k_{\text{B}}T$, then the reactions of oxide formation and oxygen desorption are suppressed, i.e., oxygen formed after oxide decomposition accumulates on the surface, but does not react with antimony to form oxide and is not desorbed, which contradicts the experiment.

There are no data in the literature on the desorption of oxygen from the surface of InSb or from the surface of indium and antimony oxides. $E_{\text{des.O}}$from the surface of metals (Au, Ag, Pt) varies from 1.19 to 1.68 eV [24,25], which corresponds to chemical adsorption. In our calculation, this $E_{\text{des.O}}$ range corresponds to the $E_{\text{form}} = 1.03-1.52$ eV range, at which the calculation describes the experiment.

5. Conclusion

In situ studied the process of thermal removal of oxide from the surface of InSb using high-speed electron diffraction. Registration of the main reflection of InSb becomes possible at a thickness of the oxide layer ~ 1 nm. The dependence of the oxide thickness on the annealing temperature and time is calculated based on the evolution of the HEED reflection intensity. The dependence of the oxide thickness on time is described using a system of equations for the reactions of decomposition and oxide formation. It is shown that the rate of oxide removal decreases when antimony flow is supplied due to the reverse reaction — oxide formation. To influence the oxide removal process, antimony and oxygen should be chemically adsorbed on the surface; physically adsorbed antimony and oxygen, even in the presence of an antimony flow and activation energies of the oxide formation reaction $\sim k_{\text{B}}T$, do not affect the oxide removal process due to the intense desorption of elements. The activation energy for the decomposition of antimony oxide was determined to be 2.17 eV at antimony desorption energies of 1.6 eV and the frequency factor $10^{13}\,\text{c}^{-1}$. The activation energies for the formation of antimony oxide (E_{form}) and oxygen desorption ($E_{\text{des.O}}$), at which the calculation describes the experiment, are determined in the ranges: $E_{\text{form}} = 1.03-1.52$ eV, $E_{\text{des.O}} = 1.19-1.68$ eV.

Conflict of interest

The authors declare that they have no conflict of interest.

References

[1] A. Evirgen, J. Abautret, J.P. Perez, A. Cordat, A. Nedelcu, P. Christol. Electron. Lett., **50** (20), 1472 (2014).
[2] M.A. Sukhanov, A.K. Bakarov, D.Yu. Protasov, K.S. Zhuravlev. Pisma v Zhurn. Tekh. Fiz., **46** (4), 3 (2020). (in Russian).
[3] J. Abautret, J.P. Perez, A. Evirgen, F. Martinez, P. Christol, J. Fleury, H. Sik, R. Cluzel, A. Ferron, J. Rothman. J. Appl. Phys., **13** (18), 183716 (2013).
[4] A.K. Bakarov, A.K. Gutakovskii, K.S. Zhuravlev, A.P. Kovchavtsev, A.I. Toropov, I.D. Burlakov, K.O. Boltar, P.V. Vlasov, A.A. Lopukhin. Zhur. Tekh. Fiz., **87** (6), 900 (2017). (in Russian).
[5] W.K. Liu, W.T. Yuen, R.A. Stradling. J. Vac. Sci. Technol. B, **13** (4), 1539 (1995).
[6] H. Simchi, S. Bahreani, M.H. Saani. Eur. Phys. J. Appl. Phys., **33** (1), 1 (2006).
[7] R. Tessler, C. Saguy, O. Klin, S. Greenberg, E. Weiss, R. Akhvlediani, R. Edrei, A. Hoffman. Appl. Phys. Lett., **88** (3), 031918 (2006).
[8] N.A. Viglin, I.V. Gribov, V.M. Tsvelikhovskaya, E.I. Patrakov. FTP, **53** (2), 277 (2019). (in Russian).
[9] E. Weiss, O. Klin, S. Grossman, S. Greenberg, P.C. Klipstein, R. Akhvlediani, R. Tessler, R. Edrei, A. Hoffman. J. Vac. Sci. Technol. A, **25** (4), 736 (2007).
[10] W. Mönch. *Semiconductor surfaces and interfaces* (Springer Science & Business Media, 2013).
[11] W.K. Liu, M.B. Santos. J. Vac. Sci. Technol. B, **14** (2), 647 (1996).
[12] J.F. Klem, J.Y. Tsao, J.L. Reno, A. Datye, S. Chadda. J. Vac. Sci. Technol. A, **9** (6), 2996 (1991).
[13] J.J. Bomphrey, M.J. Ashwin, T.S. Jones, G.R. Bell. Results Phys., **5**, 154 (2015).
[14] P.D. Brewer, D.H. Chow, R.H. Miles. J. Vac. Sci. Technol. B, **14** (3), 2335 (1996).
[15] B.R. Hancock, H. Kroemer. J. Appl. Phys., **55** (12), 4239 (1984).
[16] A. Ichimiya, P. Cohen. *Kinematic electron diffraction. In Reflection High-Energy Electron Diffraction* (Cambridge, Cambridge University Press, 2004) p. 130. doi: 10.1017/CBO9780511735097.011
[17] C.J.J. Powell.J.Vac. Sci. Technol. A, **38** (2), 023209 (2020).
[18] H. Shinotsuka, S. Tanuma, C.J Powell, D.R. Penn. Surf. Interface Anal., **51** (4), 427 (2019).
[19] S. Tanuma, C.J. Powell, D.R. Penn. Surf. Interface Anal., **43** (3), 689 (2011).
[20] W. Han, P. Huang, L. Li, F. Wang, P. Luo, K. Liu, X. Zhou, H. Li, X. Zhang, Y. Cui, T. Zhai. Nature Commun., **10** (1), 4728 (2019).
[21] Z. Wang, E.G. Seebauer. Appl. Surf. Sci., **181** (1−2), 111 (2001).
[22] J. Tao, A.M. Rappe. Phys. Rev. Lett., **112** (10), 106101 (2014).
[23] J.J. Zinck, E.J. Tarsa, B. Brar, J.S. Speck. J. Appl. Phys., **82** (12), 6067 (1997).
[24] D. Tsiplakides, S. Neophytides, C.G. Vayenas. Ionics, **3** (3), 201 (1997).
[25] N.D.S. Canning, D. Outka, R.J. Madix. Surf. Sci., **141** (1), 240 (1984).

Translated by E.Potapova